

Systematic and Causal Corrections to the Coherent Potential Approximation

M. Jarrell¹, and H. R. Krishnamurthy²¹ Department of Physics, University of Cincinnati, Cincinnati, OH 45221² Department of Physics, IISc, Bangalore 560 012, India

(February 7, 2020)

The Dynamical Cluster Approximation (DCA) is modified to include disorder. The DCA incorporates non-local corrections to local approximations such as the Coherent Potential Approximation (CPA) by mapping the lattice problem with disorder, and in the thermodynamic limit, to a self-consistently embedded finite-sized cluster problem. It satisfies all of the characteristics of a successful cluster approximation. It is causal, preserves the point-group and translational symmetry of the original lattice, recovers the CPA when the cluster size equals one, and becomes exact as $N_c \rightarrow \infty$. We use the DCA to study the Anderson model with binary diagonal disorder. It restores sharp features and band tailing in the density of states which reflect correlations in the local environment of each site. While the DCA does not describe the localization transition, it does describe the onset of localization.

I. INTRODUCTION

The Coherent Potential Approximation (CPA) is a widely used method for treating disordered systems. Within the CPA, the problem is first averaged over all possible disorder configurations in an attempt to regain the translational invariance lost due to disorder. Then non-local correlations of the disorder potential are neglected leading to a single-site approximation (like the Weiss mean field theory of magnetism). It has been applied with great success to a variety of problems [1], including ab-initio calculations in disordered metallic alloys [2].

Nevertheless, the CPA fails to provide a completely satisfactory theory for disordered alloys [1]. As a single-site mean field theory, it cannot account for the local order in the environment of each site responsible for band tailing and sharp structures in the density of states. There have been many attempts to formulate non-local corrections to the CPA in which the lattice is mapped onto a self-consistently embedded finite-sized cluster. However, these theories all fail in some significant way [1]. A successful theory must be able to account for fluctuations in the local environment in a self-consistent way, become exact in the limit of large cluster sizes, and recover the CPA when the cluster size equals one. It must be easily implementable numerically and preserve the translational and point-group symmetries of the lattice. Finally, and most signif-

icantly, it should be fully causal so that the single-particle Green function and selfenergy are analytic in the upper half plane. No presently existing cluster extension of the CPA satisfies these requirements [1].

In this manuscript, we modify the Dynamical Cluster Approximation (DCA) [3-5] to include disorder and show that the resulting formalism satisfies each of these requirements. The DCA was developed for ordered correlated systems such as the Hubbard model to add non-local corrections to the Dynamical Mean Field Approximation. In the next Section, we review the basic diagrammatic perturbation theory formalism for disordered systems. In Sec. IIIA we show that the CPA is equivalent to neglecting momentum conservation at all internal vertices of the diagrams, and in Sec. IIIB we introduce the DCA for disordered systems which systematically restores the momentum conservation relinquished by the CPA. In Sec. IV we show that the DCA satisfies each of the desired characteristics described above. In Sec. V we show results for the two-dimensional Anderson model with binary diagonal disorder. Finally in Appendix A we present an alternate way of viewing and justifying the disordered DCA algorithm developed in this paper, using the replica method of disorder averaging.

II. BASIC FORMALISM

We consider an Anderson model with diagonal disorder, described by the Hamiltonian

$$H = \sum_{\langle ij \rangle} t_{ij} C_{i\sigma}^\dagger C_{j\sigma} + \sum_j \epsilon_j C_{j\sigma}^\dagger C_{j\sigma} + \sum_i (V_i - \epsilon_i) n_{i\sigma} \quad (1)$$

where $C_{i\sigma}^\dagger$ creates a quasiparticle on site i with spin σ , $n_{i\sigma} = C_{i\sigma}^\dagger C_{i\sigma}$. The disorder occurs in the local orbital energies V_i , which we assume are independent quenched random variables distributed according to some specified probability distribution $P(V)$. The DCA formalism that we develop in this paper is valid for any $P(V)$, although for the specific calculations presented in this paper, we take $V_i = \epsilon_i$ with equal probability $1/2$ (binary disorder).

The effect of the disorder potential $\sum_i V_i n_{i\sigma}$ can be described using standard diagrammatic perturbation

theory (although we will eventually sum to all orders). It may be re-written in reciprocal space as

$$H_{\text{dis}} = \frac{1}{N} \sum_{i,j,k;k^0}^X V_i C_{k;k^0}^j C_{k^0} e^{ir_i(k-k^0)} \quad (2)$$

The corresponding irreducible (skeletal) contributions to the selfenergy may be represented diagrammatically [1] and are displayed in Fig. 1

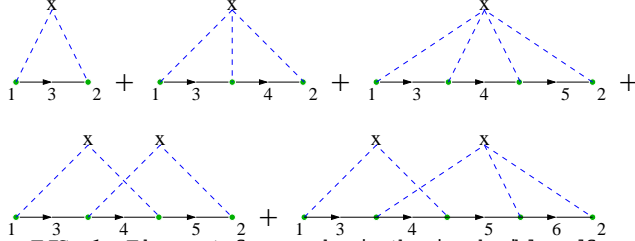


FIG. 1. The first few graphs in the irreducible self-energy of a diagonally disordered system. Each represents the scattering of a state k from sites (marked X) with a local disorder potential distributed according to some specified probability distribution $P(V)$. The numbers label the k states.

Here each X represents the scattering of an electronic Bloch state from a local disorder potential at some site represented by X . The dashed lines connect scattering events that involve the same local potential. In each graph, the sums over the sites are restricted so that the different X 's represent scattering from different sites. No graphs representing a single scattering event are included since these may simply be absorbed as a renormalization of the chemical potential.

Translational invariance and momentum conservation are restored by averaging over all possible values of the disorder potentials V_i . For example, consider the second diagram in Fig. 1, given by

$$\frac{1}{N^3} \sum_{i;k_3;k_4}^X hV_i^3 iG(k_3)G(k_4) e^{ir_i(k_3+k_4+k_2)} \quad (3)$$

where $G(k)$ is the disorder-averaged single-particle Green function for state k . The average over the distribution of scattering potentials $hV_i^3 i = hV^3 i$ independent of i . After summation over the remaining labels, this becomes

$$hV^3 iG(r=0)^2_{k_1;k_2} \quad (4)$$

where $G(r=0)$ is the local Green function. Thus the second diagram's contribution to the self energy involves only local correlations. Since the internal momentum labels always cancel in the exponential, the

same is true for all non-crossing diagrams shown in the top half of Fig. 1.

Only the diagrams with crossing dashed lines are non-local. Consider the fourth-order diagrams such as those shown on the bottom left and upper right of Fig. 1. When we impurity average, we generate potential terms $hV^4 i$ when the scattering occurs from the same local potential (i.e. the third diagram) or $hV^2 i^2$ when the scattering occurs from different sites, as in the fourth diagram. When the latter diagram is evaluated, to avoid overcounting, we need to subtract a term proportional to $hV^2 i^2$ but corresponding to scattering from the same site. This term is needed to account for the fact that the fourth diagram should really only be evaluated for sites $i \neq j$! For example, the fourth diagram yields

$$\frac{1}{N^4} \sum_{i \neq j;k_3;k_4;k_5}^X V_i^2 V_j^2 e^{ir_i(k_1+k_4+k_5+k_3)} e^{ir_j(k_5+k_3+k_4+k_2)} G(k_5)G(k_4)G(k_3) i \quad (5)$$

Evaluating the disorder average hi , we get the following two terms:

$$\frac{1}{N^4} \sum_{ijk_3k_4k_5}^X hV^2 i^2 e^{ir_i(k_1+k_4+k_5+k_3)} e^{ir_j(k_5+k_3+k_4+k_2)} G(k_5)G(k_4)G(k_3) + \frac{1}{N^4} \sum_{ik_3k_4k_5}^X hV^2 i^2 e^{ir_i(k_1+k_2)} G(k_5)G(k_4)G(k_3) \quad (6)$$

Momentum conservation is restored by the sum over i and j ; i.e. over all possible locations of the two scatterers. It is reflected by the Laue functions, $= N_{k_1+k_2}$, within the sums

$$\frac{k_2 k_1}{N^3} \sum_{k_3 k_4 k_5}^X hV^2 i^2 N_{k_2+k_4;k_5+k_3} G(k_5)G(k_4)G(k_3) + \frac{k_2 k_1}{N^3} \sum_{k_3 k_4 k_5}^X hV^2 i^2 G(k_5)G(k_4)G(k_3) \quad (7)$$

Since the first term in Eq. 7 involves convolutions of $G(k)$ it reflects non-local correlations. [Local contributions such as the second term in Eq. 7 can, if one so chooses, be combined together with the contributions from the corresponding local diagrams such as the third diagram in Fig. 1 by replacing $hV^4 i$ in the latter by the cumulant $hV^4 i - hV^2 i^2$.] Given the fact that different X 's must correspond to different sites, it is easy to see that all crossing diagrams must involve non-local correlations.

III. CLUSTER APPROXIMATIONS

A . The Coherent Potential Approximation

In the Coherent Potential Approximation (CPA), nonlocal correlations involving different scatterers are ignored. Thus, in the calculation of the selfenergy, we ignore all of the crossing diagrams shown on the bottom of Fig. 1; and retain only the class of diagrams such as those shown on the top representing scattering from a single local disorder potential. These diagrams are shown in Fig. 2.

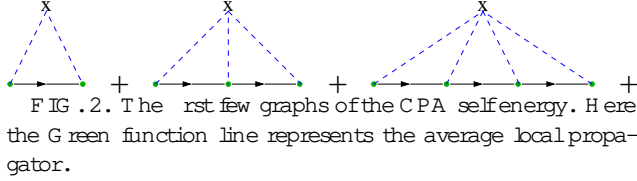


FIG. 2. The first few graphs of the CPA selfenergy. Here the Green function line represents the average local propagator.

Employing diagrammatic arguments, it is easy to see that the CPA is fully equivalent to the neglect of momentum conservation at each internal vertex. This is accomplished by setting each Laue function within the sum (eg., in Eq. 7) to 1. We may then freely sum over the internal momenta, leaving only local propagators. All non-local self energy contributions (crossing diagrams) must then vanish. For example, consider again the fourth graph. If we replace the Laue function $N_{k_1+k_4, k_5+k_3} \rightarrow 1$ in Eq. 7, then the two contributions cancel and this diagram vanishes. Thus an alternate definition of the CPA [6], in terms of the Laue functions, is

$$\Delta_{CPA} = 1 \quad (8)$$

I.e., the CPA is equivalent to the neglect of momentum conservation at all internal vertices of the disorder-averaged irreducible graphs.

B . The Dynamical Cluster Approximation

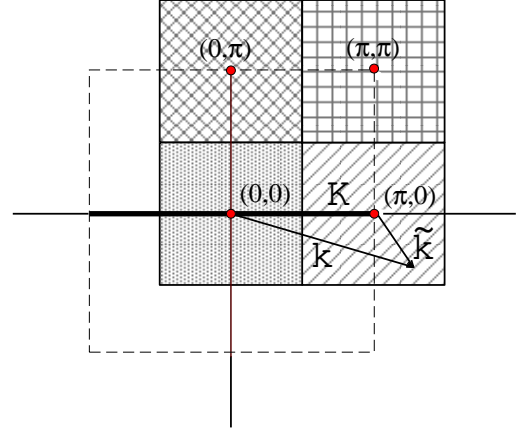


FIG. 3. $N_c = 4$ cluster cells (shown by different patterns) that partition the first Brillouin Zone (dashed line). Each cell is centered on a cluster momentum K (filled circles). To construct the DCA cluster, we map a generic momentum in the zone such as k to the nearest cluster momentum in the zone so that $\bar{K} = k - K$ remains in the cell around K .

The DCA systematically restores the momentum conservation at internal vertices which was relinquished by the CPA, and so incorporates non-local corrections. This is done by dividing the Brillouin zone into N_c equal cells, as shown in Fig. 3 and requiring that momentum be partially conserved for momentum transfers between the coarse graining cells shown in Fig. 3, but ignored for momentum transfers within each cell. This may be accomplished by employing the Laue functions

$$\Delta_{DCA} = N_c \delta_{M(k_1) + M(k_2), M(k_3) + M(k_4)} \quad (9)$$

where $M(k)$, illustrated in Fig 3, maps the momenta k to the nearest cluster momentum K . Δ_{DCA} becomes one when $N_c = 1$ since then all momenta are mapped to the zone center by M . Thus the CPA is recovered in this limit. Furthermore, as N_c becomes large, the exact result is recovered since $\lim_{N_c \rightarrow \infty} M(k) = k$ for all momenta k .

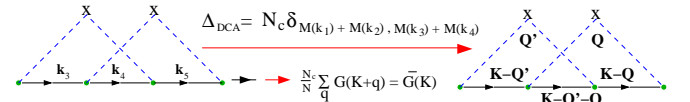


FIG. 4. Use of the DCA Laue function Δ_{DCA} leads to the replacement of the lattice propagators $G(k_1)$, $G(k_2)$, ... by coarse grained propagators $G(K)$, $G(K^0)$, ...

If we employ the DCA Laue function in each of the selfenergy diagrams shown in Fig 1 then we may freely sum over the momenta within each coarse-graining cell

shown in Fig 3. As illustrated in Fig 4 for a fourth-order graph, this leads to the replacement of the lattice propagators $G(k_1), G(k_2), \dots$ by coarse grained propagators $G(K), G(K^0), \dots$ which are given by

$$G(K) = \frac{N_c}{N} \sum_K G(K+K); \quad (10)$$

where N is the number of points of the lattice, N_c is the number of cells in the cluster, and the K summation runs over the momenta of the cell about the cluster momentum K (cf. Fig. 3).

As N_c increases from one, systematic non-local corrections to the CPA self energy are introduced. To see this, recall that the self energy is a functional of the Green function. According to Nyquist's sampling theorem [7], to reproduce correlations of length $< L=2$ in the Green function and corresponding self energy, we only need to sample the reciprocal space at intervals of $k \leq L$. Knowledge of these Green functions on a finer scale in momentum is than k unnecessary, and may be discarded to reduce the complexity of the problem. Thus the cluster self energy will be constructed from the coarse-grained average of the single-particle Green function within the cell centered on the cluster momenta. For short distances $r < L=2$, where L is now the linear size of the cluster, the Fourier transform of the Green function $G(r) = G(r) + O((r/k)^2)$, so that short ranged correlations are reflected in the irreducible quantities constructed from G ; whereas, longer ranged correlations $r > L=2$ are cut off by the finite size of the cluster [4].

We show in the appendix that that free-energy arguments presented previously [4] apply to the disordered case as well. In particular, the DCA estimate of the lattice free energy is minimized by the choice $(k;!) = (M(k);!)$.

Algorithm With the substitution $!_{DCA}$, most of the diagrams represented in Fig. 1 remain. However, the complexity of the problem is greatly reduced since the nontrivial sums involve only the cluster momenta K (numbering N_c instead of N). Furthermore, since these diagrams are the same as those from a finite-sized periodic cluster of N_c sites, we can easily sum this series to all orders by numerically solving the corresponding cluster problem. The resulting algorithm is as follows (for notational convenience the frequency arguments are not displayed below):

1. Make a guess for the impurity-averaged cluster self energy (K) , usually zero.
2. Calculate the coarse-grained cluster Green functions

$$G(K) = \frac{N_c}{N} \sum_K \frac{1}{!_{K+K}(K)} \quad (11)$$

3. Calculate the cluster-excluded propagator $G(K) = 1/(1=G(K) + (K))$. The introduction of $G(K)$ is necessary to avoid overcounting diagrams on the cluster.

4. Fourier transform G to the real space representation of the cluster problem, where the disorder potential may be represented as a diagonal matrix V , and form a new estimate of the impurity-averaged cluster Green function matrix

$$G = \frac{D}{G^{-1} - V^{-1} E} \quad (12)$$

where the average h indicates an average over disorder configurations on the cluster.

5. Transform back to the cluster reciprocal space and form a new estimate of the self energy $(K) = 1/G(K) - 1/G(K)$

6. Repeat, starting from 2, until (K) converges to the desired accuracy.

The algorithm recovers the CPA for $N_c = 1$ and becomes exact when $N_c \rightarrow \infty$.

IV. CHARACTERISTICS OF THE DCA

In Ref. [1] A. Gonis discusses the CPA, and various methods to incorporate non-local corrections. He lists the most important characteristics of a successful cluster theory. A successful theory must be able to account for fluctuations in the local environment in a self-consistent way, become exact in the limit of large cluster sizes, and recover the CPA when the cluster size becomes one. It must be straight-forward to implement numerically and preserve the full point-group symmetry of the lattice. Finally, and most significantly, it should be fully causal so that the single-particle Green function and self energy are analytic in the upper half plane. In the next two sections, we demonstrate that the DCA satisfies each of these requirements.

The limits $N_c \rightarrow \infty$ and $N_c \rightarrow 1$. As mentioned above, the DCA recovers the CPA for $N_c = 1$. As $N_c \rightarrow \infty$ it becomes exact, including correlations over all length scales. For, the DCA Laue function requires complete momentum conservation in this limit, i.e., $[K;G(K)] = [k;G(k)]$, whence $G = 1/(!_k)$ which is the bare lattice Green function so that Eq. 12 amounts to solving the problem by exact diagonalization.

Causality It is easy to show that this algorithm is fully causal [4].

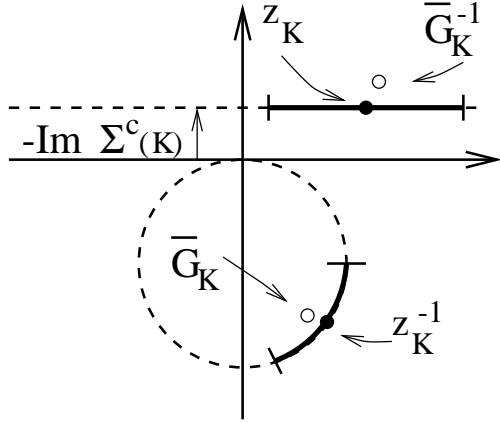


FIG. 5. Illustration of the essential steps of the proof that the DCA is causal (see text).

For our purposes, this is equivalent to requiring that all the retarded propagators and self energies are Herglotz, or analytic in the upper half plane. Since the diagrams which describe the DCA cluster problem are isomorphic to those of a real finite-size periodic cluster, the corresponding impurity averaged cluster self energy shares the causal properties of this system. Furthermore, the coarse graining step (2) cannot violate causality, since the sum of analytic functions is analytic. The only "suspect" step is the cluster-exclusion step (3), thus we must show that the imaginary part of G is negative semidefinite. The essential steps of the argument are sketched in Fig. 5. The imaginary part of $G(K;!) = (G(K;!)^{-1} + \mathcal{K}(!))^{-1}$ is negative provided that $\text{Im}(G(K;!)^{-1}) = -\text{Im}(\mathcal{K}(!))$. $G(K;!)$ can be written as $G(K;!) = (N_c=N) \sum_{\mathcal{K}} (z_{\mathcal{K}+!})^{-1}(!)$, where the $z_{\mathcal{K}+!}(!)$ are complex numbers with a positive semidefinite imaginary part $-\text{Im}(\mathcal{K}(!))$. For any \mathcal{K} and $!$, the set of points $z_{\mathcal{K}+!}(!)$ are on a segment of the dashed horizontal line in the upper half plane due to the fact that the imaginary part is independent of \mathcal{K} . The mapping $z \rightarrow 1/z$ maps this line segment onto a segment of the dashed circle shown in the lower half plane. $G(K;!)$ is obtained by summing the points on the circle segment, yielding the empty dot that must lie within the dashed circle. The inverse necessary to take $G(K;!)$ to $1/G(K;!)$ maps this point onto the empty dot in the upper half plane which must lie above the dashed line. Thus, the imaginary part of $G(K;!)^{-1}$ is greater than or equal to $-\text{Im}(\mathcal{K}(!))$. This argument may easily be extended for $G(z)$ for any z in the upper half plane. Thus G is completely analytic in the upper half plane.

Preservation of the Lattice Symmetry Since the DCA is formulated in reciprocal space, it preserves the translational symmetry of the system. However, care must be taken when selecting the coarse-graining cells to preserve the point group symmetries of the lattice. For example, the calculations presented in Sec. V are

done for a simple square lattice. Both it and its reciprocal lattice have a C_{4v} symmetry with eight point group operations. We must choose a set of coarse-graining cells which preserve this point-group symmetry. This may be done by tiling the real lattice with squares, and using the \mathcal{K} points that correspond to the reciprocal space of the tiling centers. For large V , an important conformation of the half filled system is that with all of the sites with $V_i = -V$ occupied and those with $V_i = +V$ unoccupied. To retain this conformation on the cluster, when $N_c > 1$ we will choose N_c even.

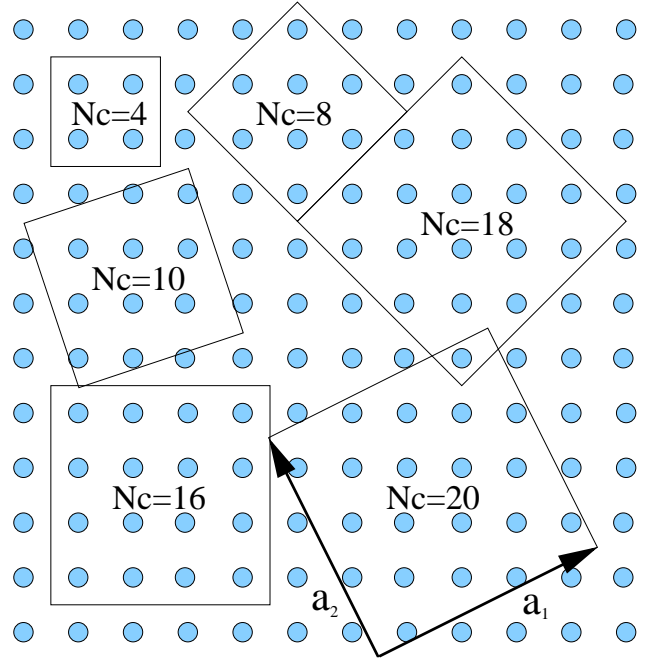


FIG. 6. Different tile sizes and orientations. The tiling principal translation vectors, a_1 and a_2 , form two sides of each tiling square (illustrated for the $N_c = 20$ tiling). For square tile geometries, $a_{2x} = a_{1y}$ and $a_{2y} = a_{1x}$.

Square tilings with an even number of sites include $N_c = 4; 8; 10; 16; 18; 20; 26; 32; 34; 36; \dots$. The first few are illustrated in Fig. 6. The relation between the principal lattice vectors of the lattice centers, a_1 and a_2 , and the reciprocal lattice takes the usual form $g_i = 2\pi a_i \cdot \hat{p}_i$ with $\mathcal{K}_{nm} = n\mathbf{g}_1 + m\mathbf{g}_2$ for integer n and m . For tilings with either $a_{1x} = a_{1y}$ (corresponding to $N_c = 8; 18; 32$) or one of a_{1x} or a_{1y} zero (corresponding to $N_c = 4; 16; 36$), the principal reciprocal lattice vectors of the coarse-grained system either point along the same directions as the principal reciprocal lattice vectors of the real system or are rotated from them by $\pi/4$. As a result equivalent momenta \mathbf{k} are always mapped to equivalent coarse-grained momenta \mathcal{K} . An example for $N_c = 8$ is shown in Fig. 7. However, for $N_c = 10; 20; 26; 34$, the principal reciprocal lattice vectors of the coarse-grained system do not point along a high symmetry

direction of the real lattice. Since all points within a coarse-graining cell are mapped to its center K , this means that these coarse graining choices violate the point group symmetry of the real system. This is illustrated for $N_c = 10$ in Fig. 7, where the two open dots, resting at equivalent points in the real lattice, fall in inequivalent coarse graining cells and so are mapped to inequivalent K points. Thus the tilings corresponding to $N_c = 10; 20; 26; 34$ violate the point-group symmetry of the real lattice system and should be avoided.

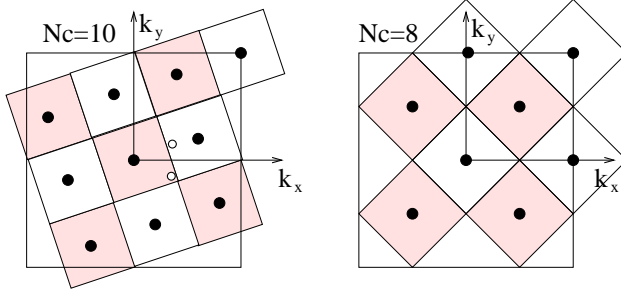


FIG. 7. The coarse graining cells for $N_c = 8$ and 10 each centered on a coarse-grained momenta K represented as black filled dots. For $N_c = 8$ equivalent momenta k are always mapped to equivalent coarse-grained momenta K . However, this is not true for $N_c = 10$ where, for example, the two equivalent momenta shown by open dots are mapped to inequivalent coarse-grained momenta.

An efficient numerical algorithm for disorder averaging. Even for a system with binary diagonal disorder, where each site can acquire only one of two values for the potential (V) the total number of disorder configurations is 2^{N_c} , which grows exponentially with N_c . For a generic quenched disorder, the probability of the various disorder configurations are determined by the specified $P(V)$; whereas, for annealed disorder, the probability of a configuration depends upon an effective Boltzmann factor determined by the electronic partition function for that particular disorder configuration [4]. In this section, we propose an approach to carrying out the disorder averaging by statistically sampling disorder configurations using a Markov process. For systems with quenched disorder, one could also sample random configurations of the disorder potentials and calculate the corresponding Green function using matrix inversion. However, a significant advantage of the Markov technique is that it may be easily modified to treat either quenched or annealed disorder [4].

In a Markov process, each disorder configuration depends upon the previous configurations. To evolve from one configuration to another, we will propose local changes in the disorder potentials. These changes are accepted with some probability determined by either the effective Boltzmann factor [4], for annealed

disorder, or the probability distribution $P(V_i)$, for quenched disorder. If we accept such a change in one of the disorder potentials, say on site l , then the new Green function matrix $G_{n,m}^0$ depends on the previous Green function matrix $G_{n,m}$ through the relationship

$$G_{n,m}^{0,1} - G_{n,m}^{-1} = V_l - V_l^0 \quad (13)$$

Since we change on the potential on the site l and the matrices V and V^0 are diagonal, their difference $V - V^0$ is a diagonal matrix with only the l 'th diagonal element finite. Then

$$G_{n,m}^0 = G_{n,m} + G_{n,l} V_l G_{l,m}^0 \quad (14)$$

If we set $l = n$ in Eq. 14, we get

$$G_{l,m}^0 = \frac{G_{l,m}}{1 - G_{l,l} V_l} \quad (15)$$

If we substitute this result back into Eq. 14, we get

$$G_{n,m}^0 = G_{n,m} + G_{n,l} \frac{V_l}{1 - G_{l,l} V_l} G_{l,m} \quad (16)$$

an equation which requires roughly N_c^2 operations to evaluate [8].

V. RESULTS

A. Single-Particle Properties

To illustrate the algorithm discussed above, we present calculations on a two-dimensional square lattice system with $t = 0.25$ and binary random disorder so that $V_i = \pm V$ with equal probability. No tricks are used to force the algorithm to remain causal such as renormalizing the spectrum or cutting off any negative tails of the density of states.

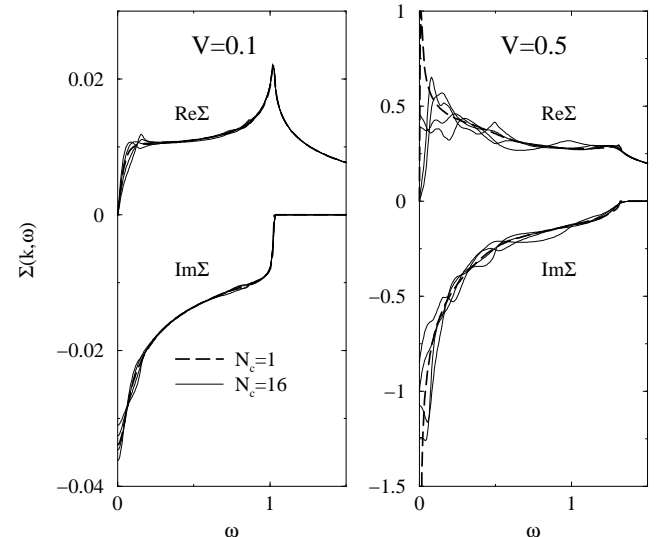


FIG. 8. The self energy $N_c = 1$ and for $N_c = 16$ for different values of K for $V = 0.1$ (left) and $V = 0.5$ (right). The thin lines show $\langle K; \omega \rangle$ for $K = (0; 0)$, $K = (0; \pi)$, $K = (\pi; \pi)$ and $K = (\pi; 0)$, plotted versus ω for $N_c = 16$. For $V = 0.1$ the self energy at the different values of K is essentially the same as the $N_c = 1$ result. For $V = 0.5$ they differ significantly, indicating that the momentum dependence of the self energy increases with V .

The self energy is plotted in Fig. 8 for $N_c = 1$ and for $N_c = 16$ for different values of K for $V = 0.1$ (left) and $V = 0.5$ (right). For $V = 0.1$ the self energy for $N_c = 16$ has very little momentum dependence, thus the different curves fall atop of one another. They also are hence very close to the self energy for $N_c = 1$ (the CPA result) indicating that it is a very good approximation for the self energy when V is small. However, for larger $V = 0.5$ the self energy curves at different values of K for $N_c = 16$ differ considerably from each other and from the self energy obtained with $N_c = 1$. Thus, as V increases non-local corrections become important and are expressed in the momentum-dependence of the self energy.

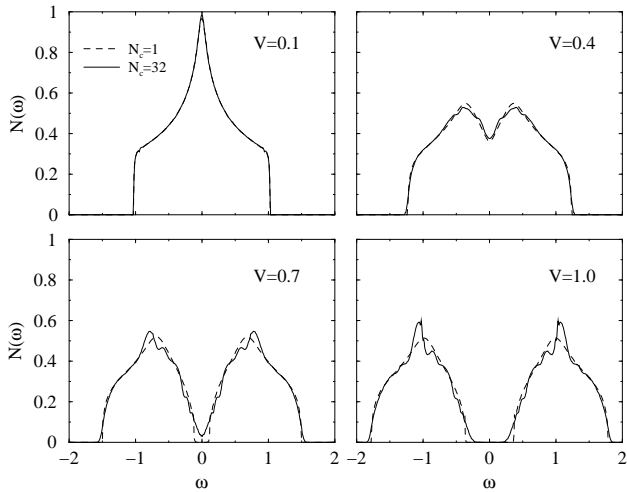


FIG. 9. The density of states for $N_c = 1$ and for $N_c = 32$ for four values of disorder potential V .

As shown in Fig. 9 (top left) the single particle density of states is essentially independent of N_c for $V = 0.1$; however, for $V = 1.0$, the density of states depends strongly upon N_c . In particular the gap around $\omega = 0$, which is sharp for $N_c = 1$, is partially filled in. The top and bottom of the band also acquire tails as N_c increases. When $N_c > 1$, the density of states acquires several additional structures which correspond to important local configurations of the disorder. The additional features and the band tails are absent in the CPA and believed to be due to local order in the environment of each site [1].

B. Localization

To test whether the DCA describes localization, we measure the probability that an electron remains at site 1 for all time [9,10]

$$P(1) = \lim_{t \rightarrow \infty} \frac{1}{t} \int_0^t \langle G(1;1;t) \rangle^2 dt = \lim_{t \rightarrow \infty} \frac{1}{t} \int_0^t \langle G(1;1;t+i) \rangle^2 dt \quad (17)$$

Since the cluster is formed by coarse-graining the real-lattice problem in reciprocal space, local quantities on the cluster and the real lattice correspond one-to-one. Thus, to test for localization, we need only apply the formula 17 for each site on the cluster. Making this substitution and introducing the local coarse-grained spectral function, $A(l; \omega) = \frac{1}{\pi} \text{Im} G(l; l; \omega)$, Eq. 17 becomes

$$P(1) = \lim_{t \rightarrow \infty} p(t) = \lim_{t \rightarrow \infty} \frac{2i}{N_c} \sum_{l_1, l_2} \int_0^t \langle A(l_1; \omega) A(l_2; \omega) \rangle dt \quad (18)$$

$p(t)$ is plotted versus t in the inset to Fig. 10 for the half-filled model when $V = 0.4$. The $p(t)$ extrapolates to zero, indicating the lack of localization.

This result can be understood from either a diagrammatic perspective or by carefully assessing the cluster problem. The crossing diagrams, especially those which involve many crossings, describe the coherent backscattering of electrons which leads to localization. [11] Thus the CPA sum over all non-crossing diagrams does not describe localization. Within the DCA, for $N_c > 1$, the crossing graphs are restored. Within each diagram, each X represents scattering from distinct site. Since there are only N_c sites on the cluster, the maximally crossed DCA graphs can have at most N_c crossings. Since all states are expected to be localized in two dimensional disordered system, apparently an infinite number of crossings are needed to describe localization diagrammatically. From the perspective of the cluster, this result is not surprising since each site on the cluster is coupled to a non-interacting translationally invariant host into which electrons can escape. Thus, if the density of states is finite at some energy, then the corresponding states can not be localized unless the hybridization rate at that energy between the cluster and the host vanishes.

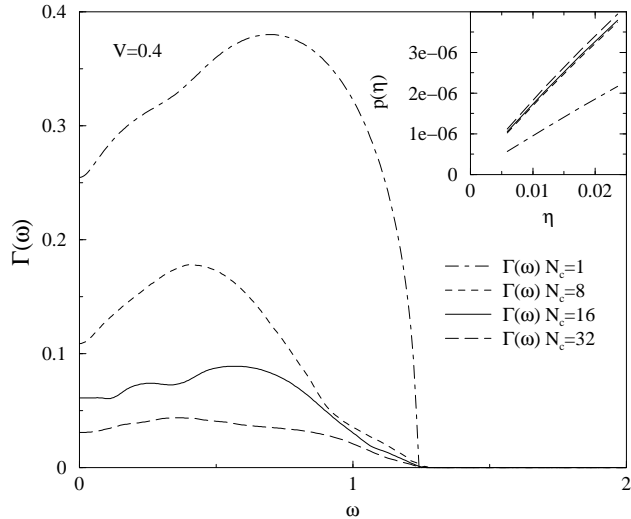


FIG. 10. The local hybridization rate when $V = 0.4$ for several values of N_c . The probability that the electron remains localized $p(\eta > 0)$, when $\eta = 0$ (half filling) is shown in the inset. As $\eta \rightarrow 0$, $p(\eta)$ extrapolates to zero indicating the lack of localization.

As described in Ref. [5], the hybridization rate between the cluster and its host is given by

$$\langle K; ! \rangle = \text{Im} \frac{1}{G(K; !)} + \langle K; ! \rangle \quad (19)$$

The net hybridization rate to a site on the cluster (the K -integrated $\langle K; ! \rangle$) is plotted in Fig. 10 when $V = 0.4$ for several values of N_c . It remains finite over the entire region where the corresponding density of states, shown in Fig. 9, is finite. This is consistent with the lack of localization demonstrated in the inset.

However, the hybridization falls as N_c increases (for large N_c , $\langle K; ! \rangle \sim 1/N_c$) [5] especially at the band edges. Furthermore the number of diagrammatic crossings increases with N_c . Thus, it is likely that the disordered DCA can describe the onset of localization. To test this, we measure the probability that an electron on a site l remains after a time t , $P(t) = \langle \mathcal{J}(l; l; t) \rangle^2$. As shown in Fig. 11, for $N_c = 1$, this probability falls quickly with time. The long time behavior is shown in the inset. As N_c increases, the electron remains localized for longer times.

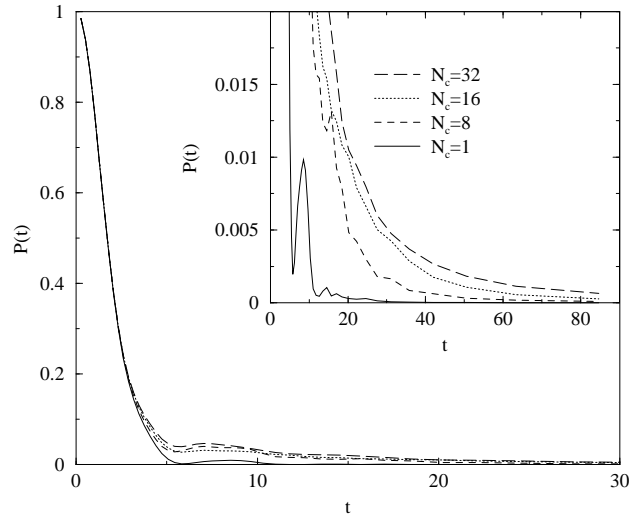


FIG. 11. The probability that an electron on a site l remains after a time t , $P(t) = \langle \mathcal{J}(l; l; t) \rangle^2$ for several values of N_c when $V = 0.4$.

V I. C O N C L U S I O N

We have developed a modification of the Dynamical Cluster Approximation to treat disordered systems. This formalism satisfies all of the characteristics of a successful cluster approximation. It is causal, preserves the point-group and translational symmetry of the original lattice, recovers the CPA when the cluster size goes to one, and becomes exact as $N_c \rightarrow 1$. Like the CPA the problem is disorder averaged and has a simple diagrammatic formulation. It is easy to implement numerically and restores sharp features and band tailing in the DOS which reflect correlations in the local environment of each site. It systematically restores the crossing graphs known to be responsible for localization. Although the DCA does not capture the localization transition, it does seem to describe the onset of localization, and might be able to access the transition itself via an appropriate finite size scaling analysis which remains to be developed.

The DCA formalism we have discussed here can also be extended to problems with disorder and interactions simply by incorporating interaction diagrams in the self energy. This is also discussed in the Appendix below. The DCA should be able to provide a good description of localization effects at finite temperatures in such contexts. For, in such cases the scattering processes are partially inelastic, so that the coherent back scattering disappears after a characteristic inelastic scattering time [12]. In this time only a finite number of back-scattering processes can occur so only a finite number of diagrammatic crossings are needed to describe the finite-temperature physics, and these are captured in the DCA.

Acknowledgments This work was initiated in conversations with B.L. Gyor'y. It is a pleasure to acknowledge useful discussions with F.P. Esposito, A.Gonis, M.Ma. This work was supported by NSF grants DM R-9704021, DM R-9357199. Computer support was provided by the Ohio Supercomputer Center.

Quantum Field Theory and Statistical Physics, (D Reidel Publishing Company, Dordrecht, Holland 1983).

APPENDIX A: DISORDER-DCA FROM THE REPLICCA METHOD

An alternate way of justifying the DCA in the context of disordered systems is to use the replica trick for disorder averaging [13]. For, this maps the disorder averaged problem into what looks like an interacting problem, whence the DCA formalism developed by us earlier [3,4] can simply be transcribed for this case, to arrive at the appropriate self consistent cluster problem. For the effective cluster problem, the replica trick can be "un-done", and we recover the algorithm presented earlier in this paper. The same procedure also works for problems involving both disorder and interactions. We detail this below.

As is well known, for problems involving quenched disorder, as for example corresponding to the Hamiltonian:

$$H = H_0 + H_{dis} \quad (A1)$$

$$H_0 = \sum_k C_k^y; C_k; \quad (A2)$$

$$H_{dis} = \sum_i V_i n_i; \quad (A3)$$

where $C_k = \sum_i C_{ki}$, and V_i is the random potential distributed according to a given probability distribution $P(V)$, complications arise because the disorder averaging has to be done on the free energy

$$F = -k_B T \ln Z$$

and the green functions

$$G_{ij}(\omega) = \text{Tr}[\langle C_{ij}(\omega) C_j^y \rangle \exp(-H)] / Z$$

Here $Z = \text{Tr}[\exp(-H)]$ is the partition function, and $\langle \dots \rangle$ represents the imaginary-time ordering operator.

In the replica trick [13], one writes

$$\ln Z = \lim_{m_r \rightarrow 0} \frac{Z^{m_r} - 1}{m_r} \quad \text{and} \quad 1/Z = \lim_{m_r \rightarrow 0} Z^{m_r - 1}$$

and assumes that the order of taking the limit $m_r \rightarrow 0$ and disorder averaging can be interchanged. Then for any positive integer m_r , the resulting disorder averaged quantities such as $\langle C_{ij}^{m_r} \rangle$, $\langle G_k(\omega) \rangle$, etc., can be represented in terms of an interacting problem involving m_r replicas of the original electronic degrees of freedom, which we index with the subscript $\alpha = 1; \dots; m_r$.

For example, using the standard Fermionic (Grassmann variable) functional integrals [14] to represent the traces above, we can write

-
- [1] For a detailed discussion of the CPA and earlier work on the inclusion of non-local corrections see A.Gonis, Green functions for ordered and disordered systems, in the series Studies in Mathematical Physics Eds. E. van Groesen and E.M.DeJager, (North Holland, Amsterdam, 1992).
- [2] B.L.Gyor'y, D.D.Johnson, F.J.Pinski, D.M.Nicholson D.M. Stocks, Alloy Phase Stability, Eds. G.M.Stocks and A.Gonis, Proc. of the Nato Adv. Study Inst. on Alloy Phase Stability, pp.421-468 (Kluwer, Dordrecht, 1987); G.M.Stocks and H.Winter, The Elec. Structure of Complex Systems, Eds.P.Phariseau and W.M.Temmeman, Proc. of the Nato Adv. Study Inst. on Electronic Structure of Complex Systems, pp.463-579. (Plenum, New York, 1982).
- [3] M.H.Hettler, A.N.Tahvildar-Zadeh, M.Jarrell, T.Pruschke, H.R.Krishnamurthy, Phys. Rev. B 58, pp.7475-7478 (1998).
- [4] M.H.Hettler, M.Mukherjee, M.Jarrell, H.R.Krishnamurthy, Phys. Rev. B 61, 12739 (2000).
- [5] Th.Maier, M.Jarrell, Th.Pruschke, and J.Keller, Eur.Phys.J.B 13, 613 (2000)
- [6] This same substitution was shown to serve as a diagrammatic definition of the Dynamical Mean Field (in finite-dimensional) Theory, see E.Muller-Hartmann, Z.Phys.B 74, 507 (1989); 76, 211 (1989). The CPA becomes exact in the limit of infinite dimensions, see R.Vlamming and D.Vollhardt, Phys. Rev. B 45, 4637 (1992).
- [7] see D.F.Elliott and K.R.Rao, Fast Transforms: Algorithms, Analyses, Applications, (Academic Press, New York, 1982).
- [8] J.E.Hirsch and R.M.Fye, Phys.Rev.Lett. 56, 2521 (1986).
- [9] A.J.McKane and M.Stone Annals of Physics 131, pp36-55 (1981).
- [10] D.J.Thouless, Physics Reports, 13c, n.3, 94, (1974).
- [11] P.A.Lee and T.V.Ramakrishnan, Rev.Mod.Physics, 57, n.2, 287, (1985).
- [12] G.Bergmann, Physics Reports 107 no 1, p1-58 (1984)
- [13] F.Wegner, Z.Phys.B 35 207 (1979); L.Schafer and F.Wegner, Z.Phys.B 38 113 (1980); K.B.Efetov, A.I.Larkin and D.E.Khemelnitskii, Sov. Phys. JETP 52,568 (1980); A.A.M.Pruisken and L.Schafer, Nucl. Phys B 200, 20 (1982).
- [14] For example, see V.N.Popov, Functional Integrals in

$$\ln Z^{m_r} = \int \mathcal{D}c \mathcal{D}c \exp [\dots] \quad (A4)$$

$$\ln G_k(i) = \int \mathcal{D}c \mathcal{D}c c_{k; ; 1} () c_{k; ; 1} (0) \exp [\dots] \quad (A5)$$

Here is an effective free energy functional which arises from the disorder averaging, and can be written as

$$= \int_{k; ; 0}^X \int^Z d c_{k; ; ()} (\otimes + k) c_{k; ; ()} + \int_i^N W(\mathfrak{n}_i) \quad (A6)$$

where,

$$\mathfrak{n}_i = \int_{; 0}^X \int^Z n_{i; ; ()} d$$

and

$$\exp [W(\mathfrak{n}_i)] = \int \exp (V_i \mathfrak{n}_i) = \int dV_i P(V_i) \exp (V_i \mathfrak{n}_i)$$

In terms of the cumulants V^1_c of the disorder distribution $P(V)$, one can write

$$W(\mathfrak{n}_i) = \sum_{l=2}^X \frac{1}{l!} V^l_c (\mathfrak{n}_i)^l$$

So, clearly, W introduces (local in space but non-local in time) interactions between electrons belonging to arbitrary replicas.

If one re-expands $\exp [W(\mathfrak{n}_i)]$ in powers of the cumulants V^1_c one can perform the Fermionic traces using the standard techniques of diagrammatic perturbation theory. Then, order-by-order in perturbation theory, the dependence on m_r is explicit and analytic, and the $\lim_{m_r \rightarrow 0}$ can be evaluated precisely. The resulting terms are in exact, one-to-one correspondence with the terms obtainable by writing out the diagrams from a direct perturbation expansion in powers of V_i and then disorder averaging as discussed in Section II. The $m_r \rightarrow 0$ limit eliminates the diagrams (in the interacting problem) containing internal loops with free sums over the replica indices (as required, since such diagrams never appear in the direct disorder averaged perturbation theory formalism of Section II).

For the "replicated interacting problem" obtained above, one can transcribe exactly the DCA formalism discussed in refs. [3,4]. If one assumes that the self-consistent host propagators do not break replica symmetry, then the effective cluster problem corresponds to a Fermionic functional integral involving an effective, self-consistent cluster free energy functional given by

But, as is easy to see using the same procedure as outlined earlier in this appendix, such an effective free energy functional is exactly what one would obtain if one were to disorder average (using the replica trick) a cluster problem with N_c sites which are dual to the cluster momenta K , a bare (retarded) cluster propagator $G^1(K; 0)$, and a random potential V_i distributed according to $P(V_i)$ at every site i of the cluster. Hence we have an alternate justification for the disorder-DCA algorithm set down in Section III. The above route also enables one to quickly extend our discussions in ref. [4] regarding the 2-particle propagators, W and identities, etc., to the disorder-DCA context. Most significantly, the DCA estimate of the lattice self energy is minimized by the choice $(k; !) = (M(k); !)$.

We note that the arguments presented in the main text and in this appendix are also easily extended to problems involving interactions and disorder. For example, for the case of the Hubbard model with diagonal disorder, one would add to the starting Hamiltonian the interaction term $U \sum_i n_{i; ;} n_{i; ;}$. Going through exactly the same procedures as outlined above, it is not hard to see that the only change is that the effective free energy functionals for the lattice and the cluster pick up the additional terms $U \sum_i n_{i; ;} n_{i; ;}$ and $U \sum_{i \neq j} n_{i; ;} n_{j; ;}$. The resulting cluster problem now has both interactions and disorder on the cluster of N_c sites which are dual to the cluster momenta K : a bare (retarded) cluster propagator $G^1(K; 0)$, a random potential V_i distributed according to $P(V_i)$, and the Hubbard interaction U at every site i of the cluster. One can resort to any technique of one's choice to solve this problem for the disorder-averaged cluster Green functions $G(K; !)$ and cluster self-energies $(K; !)$ and go through with the rest of the DCA iteration.